Mechanism of noise generation from a modular expansion joint under vehicle passage

K.A. Ravshanovich[a], H. Yamaguchi[a*], Y. Matsumoto[a], N. Tomida[a] and S. Uno[b]

[a] *Dept. of Civil and Environmental Eng., Saitama University, Sakura-Ku, Saitama, 338-8570, Japan*
[b] *Kawaguchi Metal Industries CO. LTD, Miya-Cho, Kawaguchi, 332-8502, Japan*

Abstract

The mechanism for the generation of noise from a modular expansion joint in a bridge under vehicle passage, which can cause an environmental problem, is investigated in experiments on a full-scale model of the joint. Noise and vibration characteristics of the joint model in the near field are identified by a series of car-running experiments associated with separate tests of the acoustic and dynamic characteristics of the joint. A modal analysis based on finite element modeling of the joint is also conducted and structure-borne noise radiation is discussed by correlating the dominant frequency components of the noise with the modal parameters. It is concluded that the noise from the top of the joint, dominant in the frequency range from 500 to 800 Hz, is caused by a sudden change in the pressure of air within the gap formed by the rubber sealing with two adjacent middle beams, and that the noise from the bottom, dominant in the frequency range below 200 Hz, is attributed mainly to sound radiation from the vibration of the middle beams.

Keywords: Modular expansion joint; Noise generation mechanism; Car-running experiment; Acoustic test; Impact test; Modal analysis

1. Introduction

It is known that noise is radiated when vehicles travel at high speed over highway bridges. There are two components of noises or sounds; one is "joint sound", which is radiated when moving vehicles pass over the expansion joints of bridges and another is "span sound", which is radiated when vehicles run through the spans. Both sounds, to some extent, exert physical, physiological and psychological effects on the inhabitants around highway bridges. These effects have been considered to be environmental noise problems, and a number of studies have been reported for the case of span sound [1–3], while the studies focusing on the joint sound are rather limited.

Today's long cable-supported bridges require expansion joint systems capable of bridging gaps in the range of meters. Furthermore, the recent, frequent applications of base-isolated viaducts in highway bridges require the capability to allow multi-directional movement in both translation and rotation. To cope with this, a type of expansion joint, the modern modular-type expansion joint, which divides the total movement capacity into several small gaps by the use of steel middle-beams, has been developed and the number of applications has increased [4]. The modular expansion joint is advantageous for many reasons such as: water-tightness, cleaning requirements, geometric adaptability, and most importantly, translational and rotational motion capacity. It can accommodate the three-dimensional movements without generating additional stresses or strains in the load-bearing members or in adjacent bridge or abutment structures. Apart from its advantages, it has been recognized that the noises generated by vehicle passage over the modular joints tend to be louder than those of ordinary expansion joints [5]. Although possible techniques have been reported

* Tel & Fax: +81-48-858-3552, E-mail: hiroki@post.saitama-u.c.jp

[6] for solving the noise problem by welding or bolting sinusoidal and rhombus-shaped steel plates on top of the steel middle-beams of the modular joints, those techniques have not been successfully implemented in real applications. The difficulty can be attributed due to the fact that the joints are intensively loaded by the wheels of passing vehicles, which makes them subject to heavy dynamic loading causing fatigue mainly on connection parts of the modular joint [7]. This leads to cracking of the welded connections and weakening of the bolted connections. Accurate determination of possible sources of noise generation gives an opportunity to devise appropriate counter measures.

The authors' research group has therefore been studying the characteristics of noise generation and its control for the modular expansion joints [8, 9], and the present paper focuses on a possible mechanism of noise generation specific to the modular expansion joints. A series of car-running experiments with a full-scale model of a joint is conducted to identify the noise and vibration of the joint model in the near field when a car runs over it. The acoustic and dynamic characteristics of the joint are also investigated by experimental modal analysis in the separate tests as well as by modal analysis based on finite element modeling of the joint, hereinafter called the 'theoretical modal analysis' in order to distinguish it from 'experimental modal analysis'. Finally, possible sources of noise and structure-borne noise radiation are discussed by correlating the dominant frequency components of noise with the acoustic characteristics and the modal parameters of the joint.

2. Car-running experiment with full-scale model of modular expansion joint

2.1 Full-scale model

Figure 1 shows the full-scale model of the modular beam-grid joint used in the experiments. The model was set up in the compound of Kawaguchi Metal Industries Co., Ltd. in Saitama, Japan. The model consists of three steel I-beams aligned normal to the direction of car-running line (i.e., the middle beams), that are elastically supported by four steel I-beams aligned parallel to the direction of running line (i.e., the support beams) through the polyamide bearings and pre-stressed rubber bearings. The support beams are also supported by the polyamide bearings and fixed with pre-stressed rubber bearings in order to make the joint system movable. Control mechanisms, each consisting of a steel plank (i.e., the control beam) and two rubber elements (i.e. the control springs), provide elastic restriction of excessive relative displacement between the middle beams. The gap is made watertight by means of a non-load-carrying rubber sealing fixed between the middle beams. The whole system, therefore, behaves as a sort of 'accordion'. The cross-section properties of the beams and the spring constants of the bearings are summarized in Tables 1 and 2, respectively. It is noted that the element-test data were used for the spring constants of the bearings in their principal directions, while those in other directions were estimated semi-analytically by assuming the ratio of the spring constants between the intended direction and the principal one to be the analytical value of the cylindrical homogeneous-body model of the bearing.

The full-scale model is mounted on top of a test pit (Fig. 2) that models a space under the bridge girders. The surfaces of the pit are covered by sound absorbing materials so as to reduce the reflection of sound inside the pit, which is made of concrete.

2.2 Noise and vibration measurements

Noise generated from the joint model described above was measured in the near field when a car ran over it. The car used in the experiment was an ordinary sedan-type two-axle car whose weight and width are roughly 2000 kg and 1.65 m, respectively. The speed of the car was controlled at 50 km/h during the passage over the joint. It should be noted that the selection of the type of car and its speed were limited by the safety requirements for an experiment in the company compound.

The car-running positions were over the two centre support beams and over the two control beams at the mid-spans, as illustrated in Fig. 3, corresponding to two wheels of the car.

The sound pressure was measured above and below the joint model. The position of the sound measurement above the joint is at 0.5 m away from the left edge of the car-running position at a height of 0.5 m. The sound pressure below the joint was measured inside the test pit at 1.0 m below the top surface of the centre of the joint. The sound pressures were measured with sound level meters (RION NL-21, NL-32).

The vibration of the middle beam induced by the passage of the car was also measured along with the noise measurement. As shown in Fig. 3, the accelerations at five positions in the third middle beam were measured with piezoelectric accelerometers (RION PV-85), in the vertical direction as well as in the lateral direction that is defined to be normal to the axis of the middle beam.

Signals from the sound level meters and the accelerometers were digitized at 10000 samples per second after anti-aliasing filtering.

The set of noise and vibration measurements was repeated five times in the car-running experiment to investigate the repeatability of the measurements.

2.3 Analysis of measured data

Spectral analysis was conducted off-line for the time-series data of noise and vibration recorded in the experiment. Figure 4 shows, as an example, a set data of time series of the noises below and above the joint as well as the lateral and vertical vibrations at the center of the third middle beam. As can be seen in the figures, there are two impulsive and transient responses starting around the times of 0.17 sec and 0.35 sec, which correspond to the passages of the front and rear axles of the car, respectively. It is noted that the very low frequency component observed in Fig. 4 (b) is the change in air pressure caused by the car running through the vicinity of the sound level meter above the joint. The transient records for the period of the first 0.6 sec in Fig. 4 were used in the spectral analysis by applying the Fourier transform with the scan averaging method [10]. That is, the Fourier spectrum was obtained by scanning a Hanning window of length T (= 0.4096 sec) over the entire record; this was done in overlapping steps with step length T/4, and the results were averaged. The frequency resolution of the spectral data is therefore 2.44 Hz.

The eigensystem realization algorithm (ERA) [11] was also applied to the free vibration part of the acceleration record for the period of 0.48 sec from the termination time of rear axle's impact load, which is around 0.39 sec in Figs. 4 (c) and (d). All the acceleration records at the five measuring points of the third middle beam were simultaneously analyzed by the ERA in order to extract the dominant components of the joint excited by the car running, which are not only the dominant frequencies but also the associated response-mode shapes and damping ratios. The size of the Hankel matrix in the ERA analysis was selected as 4000 x 800 after some trials to check the stability of the result.

3. Characteristics of noise and noise generation mechanism

Figures 5 and 6 show the full result on noises of the five measurements for both the car running over the control beams and the car running over the support beams. In the frequency range above 1000 Hz (not shown in the figures), there were no dominant frequency components in the noise and vibration. It is also noted that the sound pressure below 20 Hz is omitted in the figures simply because the frequency range of the sound level meters was from 20 Hz to 20 kHz. It was found that the repeatability of the measurement was relatively low in the noise above the joint, particularly in the frequency range between 500 and 800 Hz (Fig. 5). This may imply that the noise

above the joint may have been more vulnerable to variations in the measurement, such as a possible variation in the position and speed of the car. Figures 5 and 6 also show that the characteristics of the noise measured above the joint are different from those of the noise below the joint. The noise above the joint shows large peaks in the frequency range between 500 and 800 Hz with a variation among measurements, while the noise below the joint has dominant frequency components in the relatively low frequency range below 500 Hz.

3.1. Noise above joint

As is clearly shown in Fig. 5, the noise above the joint has dominant frequency components in the frequency range from 500 to 800 Hz. Although there are some dominant components at lower frequencies, the noise in that frequency range may make a major contribution to the environmental noise problem, because the sensitivity of the human ears decreases with decreasing frequency in the range below 800 Hz [12].

In order to find a possible source of the noise in that frequency range, the acoustic characteristics of the joint's gap was investigated experimentally. The acoustic test of the joint showed that the air in the gap formed by the rubber sealing with two adjacent middle beams had a resonance at around 700 Hz when the top was covered by a car tire [8, 9]. Although the details of the test are not explained in this paper, the sound pressures measured with and without covering the top of the gap by a car tire are compared, so that the effect of the cover is represented by a frequency response in the amplification factor, as depicted in Fig. 7. The results shown in Fig. 7 illustrate a resonance at frequencies around 700 Hz with a variation between different sizes of tire for different types of car; sedan and wagon. This variation in the acoustic resonance frequency due to the tire size may be consistent with the vulnerability of the noise above the joint to variations in the measurement, previously considered in Fig. 5.

The effects of the noise control measures were also investigated in the car-running experiment [8, 9]. One of the noise control measures proposed when the study was conducted was an installation of fillings for the gaps formed by the rubber sealing with two adjacent middle beams. Figure 8 shows the spectra of the noise measured above the joint with and without the fillings made from a rubber material for the gaps. It shows that the sound pressure clearly decreased in the frequency range between 500 and 800 Hz.

From the above discussions, it can be concluded that the noise above the joint in the frequency range between 500 and 800 Hz is attributed to a sudden change in the air pressure, that is a compression, within the gap formed by the rubber sealing with the two adjacent middle beams when a car ran over the gap.

3.2. Noise below joint

As shown in Fig. 6, the noise below the joint has dominant frequency components below 500 Hz, especially at around 70 Hz, 80 Hz, 140 Hz, 160 Hz in both cases of car running (Figs. 6 (a), (b)) and only 270 Hz when the car ran over the support beams (Fig. 6 (b)).

As for the corresponding accelerations measured in the third middle beam, the spectra of the lateral and vertical accelerations at the beam center are depicted in Fig. 9 for the five measurements in both cases of the car running over the control beams and over the support beams. A stabilization diagram of the ERA analysis for one measurement, which represents the natural frequencies identified with respect to the model order, is also given in each figure. Among the very many natural frequencies identified by the ERA, only the more accurate values with a modal amplitude coherence γ [11] larger than 0.999 are plotted. Because the ERA analysis was simultaneously applied to all the acceleration records at the five measuring points of the third middle beam, the frequencies of the modes that have a node close to the beam center can also be identified in the

stabilization diagrams, while those frequencies cannot have significant peaks in the spectra of accelerations at the beam center. Figure 9 shows that the contributions to the structural responses are mainly in the frequency range below 500 Hz, and that the lateral accelerations are more than five times greater than the vertical accelerations, particularly at dominant frequencies below 150 Hz. The dominant and stable frequency components are found in the spectra and/or in the stability diagrams at 70 to 80 Hz, 110 to 120 Hz, 220 to 230 Hz in both the lateral and vertical directions, at 370 to 400 Hz mainly in the lateral direction, at about 150 Hz and 180 Hz mainly in the vertical direction.

The vibration modes associated with these dominant frequencies were also identified by the ERA analysis and are depicted in Figs. 10 and 11 for the lateral and vertical vibrations, respectively. In each figure, the modal amplitudes for different model orders in the ERA are plotted at the five measuring points of the third middle beam in order to represent half of the response mode shape in the third middle beam. It can be seen that the response mode shapes are partially identified showing the different shapes of deflection for the different frequencies in the responses induced by the running of the car. More detailed discussion on the response modes, however, is to be done in *5.3* after identifying the full mode shapes of the modular expansion joint by modal analysis.

It should be noted that the damping ratios associated with those dominant and stable frequency components are also stably identified and relatively low in magnitude, as shown in Fig. 12, where the damping ratio is plotted with respect to the frequency for the model order up to 100 under the condition of modal amplitude coherence $\gamma > 0.999$, corresponding to the stabilization diagram in Fig. 9. This means that the dynamic response characteristics identified in the car-running experiment are reasonably accurate.

In order to directly compare the noise below the joint with the acceleration of the middle beam, the spectra for two cases of car running are combined and enlarged into the frequency range up to 500 Hz for the noise, lateral and vertical accelerations in Fig. 13. Because the noise below the joint must be more or less affected by the space of the test pit, the acoustic characteristics of the test pit was also investigated experimentally. The transfer function from a white-noise input induced by a speaker to a sound-pressure output measured by the sound level meter was obtained as an amplification factor for the test pit and was superimposed on the noise spectra in Fig. 13 (a). Figures 13 (a)–(c) show that most of the dominant frequency components in the noise below the joint are associated with the dominant frequency components in the vibrations of the middle beam and also with local peaks in the acoustic characteristics of the test pit. That is, the components of noise at 70 to 80 Hz and at 140 to 160 Hz are very large corresponding to the components of the accelerations in both directions and mainly in the vertical direction, respectively, while the amplification factors of the test pit at those frequencies are not necessarily very large. The dominant noise at around 270 Hz, however, might be due to the acoustic resonance in the test pit, because the amplification factor has a very large peak at that frequency in Fig. 13 (a) while there is no very dominant component in the accelerations in Figs. 13 (b) and (c). The dominant frequency component of noise at 270 Hz is significant only in the case of the car running over the support beams, as previously seen in Fig. 6, and this might be consistent with the fact that acoustic resonance is more significant for a more rigid boundary.

These observations imply that the essential frequency components in the noise below the joint are attributed mainly to the vibration of the structural elements of the modular expansion joint.

4. Experimental and theoretical modal analyses of the full-scale model joint

In order to grasp the physical meaning of the vibration response modes measured in the car-running experiment (Figs. 10 and 11), which can be considered as sources of the essential

frequency components in the noise below the joint, the natural frequencies and mode shapes of the full-scale model joint were identified both experimentally and analytically by conducting an impact test and a finite element analysis, respectively.

4.1 Experimental modal analysis by impact testing

An impact test was conducted on the joint model so as to understand the dynamic characteristics of the joint structure. Impact force was applied, by an impact hammer (Kistler 9728A20000) that had a hammerhead (weighing 1.50 kg) with a soft tip, to the third middle beam above the control beam (that is at the center of the third middle beam) and the second support beam. The acceleration responses in both the lateral and vertical directions were measured at nine locations in the same beam, as shown in Fig. 3, for the impacts in the vertical direction as well as those inclined to the lateral direction. Each impact test was repeated twice. Figure 14 shows an example of a recorded time series of acceleration. The methods of data acquisition and data analysis were the same as those in the case of the car-running experiment except that the acceleration records at nine measuring points for the period of the first 0.24 sec were used for the ERA analysis of the impact testing.

Figure 15 shows the spectra of the lateral and vertical acceleration responses at the center of the third middle beam to the impacts. Each figure contains four line plots of spectra corresponding to two measurements for the two different locations of impact, as well as a stabilization diagram of the ERA analysis under the condition of modal amplitude coherence $\gamma > 0.999$. Figure 15 shows that the natural frequencies of the model joint structure are stably identified by both the clear peaks in the spectra and the stabilization plots in the ERA result, especially in the frequency range below 200 Hz. The natural frequencies and mode shapes identified by the impact testing will be discussed in *5.1*, with those identified by the finite element analysis.

4.2 Theoretical modal analysis by finite element method

A three-dimensional finite element model of the full-scale test joint was developed in ANSYS [13] as shown in Fig. 16. The thin-walled middle and support beams were modeled as two-node beam elements having three translational, three rotational and one warping degrees-of-freedom (DOFs) at each node, while the warping was not considered for the structural members with a solid cross-section such as the control beam. All the bearings were modeled as two-node translational and rotational spring elements in all three directions, which were placed appropriately in the space by introducing auxiliary elements as also depicted in Fig. 16. In summary: the full finite element model consists of 487 beam elements, 348 spring elements and 24 mass elements. As a result, 517 nodes, 564 elements and 3191 active DOFs were recognized in the model.

5. Modal parameters of joint structure and structure-borne noise

5.1 Natural frequencies and mode shapes of full-scale model joint

The mode shapes dominated in the lateral and vertical directions, which correspond to the natural frequencies identified by the impact test in Fig. 15, as shown in Figs. 17 and 18, respectively. Experimentally and analytically identified mode shapes with natural frequencies are compared in both figures. It should be noted that, because of the symmetric structure of the modular joint, the eigenvalue problem in the analysis was degenerate in the sense that there were some sets of pairs of modes whose frequencies were very closely spaced, and that those modes were linearly combined into a more realistic mode and depicted in Figs. 17 (a), (d), 18 (a) and (b). It is obvious from Figs. 17 and 18 that the experimental mode shapes are very stable with respect to the model

order in the ERA and fairly consistent with the analytical mode shapes. The corresponding natural frequencies are also in good agreement in the case of the vertical bending dominant modes in Fig. 18, while the analytical natural frequencies of the lateral bending dominant modes are 20% smaller than the experimental ones in most cases. One of the possible reasons for this discrepancy in the natural frequency might be some difference in the condition of the connection bearings (slip or non-slip) and/or some error in the evaluation of the spring constants for the models of the bearings, which could affect on the stiffness of the joint structure more significantly in the lateral direction. The lateral stiffness of the rubber bearing in the modular joint, for example, might have frequency-dependent characteristics [14].

5.2 Discussion of the dominant vibration responses in the car-running experiment

Because of the structural complexity of the modular beam-grid joint, very many vibration modes (119 modes in total) were numerically obtained by the finite element analysis in the range of natural frequencies below 500 Hz. A modal participation factor (MPF) was, therefore, calculated for each vibration mode in order to check the modal contribution to the joint's vibration induced by the car running. The MPF in this paper is defined as the modal response at the center of the third middle beam induced by a set of two unit impulse forces on the car-running position (Fig. 3):

$$MPF \equiv \frac{\boldsymbol{\phi}_n^T \mathbf{r}}{\omega_n M_n} \tag{1}$$

where ω_n, $\boldsymbol{\phi}_n$, $M_n = \boldsymbol{\phi}_n^T \mathbf{M} \boldsymbol{\phi}_n$ ($\mathbf{M}$: the mass matrix) are the n-th natural frequency, mode vector, modal mass of the modular joint, respectively, and $\mathbf{r}$ is a force distribution unit vector. It should also be noted that the mode vector is normalized with respect to the modal amplitude at the center of the third middle beam.

Figure 19 shows the plots of the MPF with respect to the natural frequency for the lateral and vertical unit impulse forces applied to the positions as the vehicle ran over the control beams and support beams. The correspondence of these modal contribution distributions with the spectra of the car-induced acceleration response in Figs. 13 (b) and (c) are very good especially in the case of the vertical response, while there is some shift in frequency in the case of lateral response, caused by the error in the analysis of the natural frequency, as previously discussed.

A similar discussion can be made by more direct comparison of the dominant response modes in the car-running experiment in Figs. 10 and 11 with the identified mode shapes in Figs. 17 and 18. That is, in the case of vertical vibrations, most of the dominant frequencies (82 Hz, 113 Hz, 152 Hz, and 179 Hz) and response modes of car-induced vibration in Fig. 11 are fairly consistent with the corresponding natural frequencies and mode shapes identified both experimentally and analytically in Fig. 18. In the case of lateral vibrations, however, even the natural frequencies identified by the impact testing are not necessary equal to the dominant frequencies in the car-running experiment and the corresponding mode shapes in Fig. 17 are somewhat different from the response modes in Fig. 10. These differences in the frequency and the mode for the lateral vibrations may be caused by possible changes in the connection and boundary conditions due to the differences in the magnitude of the vibration and of the effects of the car on the joint, which are more sensitive in the lateral direction. In fact the modal damping ratios of the lateral vibration mode, identified by the impact testing, fluctuate more than those of the vertical vibration mode, as shown in Fig. 20, and differ from the damping ratios identified in the car-running experiment in Fig. 12 (a).

According to the above discussions, it is concluded that the dominant frequency components in the acceleration responses observed in the car-running experiment can be related to the vibration

modes of the joint structure, however, a more precise investigation of the lateral response behavior of modular joint remains to be done.

5.3 Discussion of structure-borne noise radiation in the car-running experiment

As previously discussed in *3.2*, the components of noise below the joint at 70 to 80 Hz and at 140 to 160 Hz are most dominant, corresponding to the large components of the acceleration responses. Because the dominant components of the acceleration responses can be related to the vibration modes of the joint structure, as concluded in *5.2*, the corresponding mode shapes of the whole joint in three dimensions are depicted in Fig. 21. It is seen in Fig. 21 that all the vibration modes corresponding to the dominant frequency components in the noise below the joint are classified as a type of mode in which all the middle beams dominantly vibrate in the vertical and lateral directions with large amplitudes. The result of the eigenvalue analysis shows another type of mode in which the bending vibrations of the support beams are dominant. It is therefore concluded that the noise measured below the joint is caused by the sound radiation due to the bending vibration modes of the middle beams induced by an impact from the car wheels.

6. Conclusions

A possible source for, and mechanism of, the noises generated from the modular-type bridge expansion joint under vehicle passage was investigated by conducting the car-running experiment with a full-scale model of a joint, associated with the acoustic tests of the joint spaces, the impact test and the finite element analysis of the joint structure. The main conclusions derived in this study are summarized as follows:

1) The noise generated above the joint is dominated by frequency components in the frequency range from 500 to 800 Hz, which is attributed to a sudden change in the air pressure within the gap formed by the rubber sealing with the two adjacent middle beams when a car runs over the gap.
2) The noise generated below the joint is mainly dominated by the frequency components in the frequency range below 200 Hz, which is caused by the sound radiation due to the bending vibration modes of the middle beams being excited by an impact force from the car wheels.
3) The noise generated below the joint can be significantly affected by the acoustic characteristics of the space below the joint in the sense that there is a possibility of acoustic resonance in the space.
4) The dominant frequency components of the joint vibration in the car-running experiment can be related to the numerically obtained vibration modes of the joint structure in the finite element analysis. A more precise investigation of the lateral response behavior of the modular joint remains to be done.

The present study focuses attention on the mechanism of noise generation based on the experimental data of a full-scale joint model, and will be followed by field measurements of the vibrations and noises of a prototype bridge with a modular expansion joint in order to clarify the quantitative characteristics of the noise generated from the modular joint.

Acknowledgements

This study was conducted in collaboration with Kawaguchi Metal Industries Co., Ltd. The support of Mr. Hishijima, Mr. Hiromoto, Mr. Kohara and Mr. Ozawa from that company is gratefully acknowledged.

References

[1] Goroumaru H., Shirashi K., Hara H. and Komori T.: Prediction of low frequency noise radiated from vibrating highway bridges, *Journal of Low Frequency Noise and Vibration*, **6**(4), pp.155-166, 1987.

[2] Chanpheng T., Yamada H., Miyata T. and Katsuchi H.: Application of radiation modes to the problem of low-frequency noise from a highway bridge, *Applied Acoustics*, **65**, pp.109-123, 2004.

[3] Imaichi K., Tsujimoto R., Takahashi S. and Kitagawa K.: Theoretical analysis of sound radiated from vibrating bridge, *Proceedings of Japan Society of Mechanical Engineering (part C)*, **46**(408), pp.904-12, 1980 (in Japanese).

[4] Moor G.: New joints for old, *Bridge Design & Engineering*, No.23, pp.80-81, 2001.

[5] Ramberger G.: *Structural bearings and expansion joints for bridges*, Structural Engineering Documents 6, IABSE, Zurich, Switzerland, 2002.

[6] Fobo W.: Noisy neighbors, *Bridge Design & Engineering*, No.35, p.75, 2004.

[7] Steenbergen M.J.M.M.: Dynamic response of expansion joints to traffic loading, *Engineering Structures*, **26**, pp.1677-1690, 2004.

[8] Matsumoto Y., Yamaguchi H., Tomida N., Kato T. and Ravshanovich K.A.: Noise generated from modular expansion joint – mechanism and control, *Proc. of Joint Seminar between Thammasat Univ. and Saitama Univ., March 2006, Thailand*, pp.112-121, 2006.

[9] Matsumoto Y., Yamaguchi H., Tomida N., Kato T., Uno S., Hiromoto Y. and Ravshanovich K.A.: Experimental investigation of noise generated by modular expansion joint and its control, *Journal of the Japan Society of Civil Engineers*, Division A (accepted, in Japanese).

[10] Harris C.M. (Editor in Chief): *Shock and Vibration Handbook*, 4th ed., pp.14.25-26 (FFT Analysis of Transients.), McGraw-Hill Co., Inc., 1995.

[11] Juang J.N. and Pappa R.S.: An eigensystem realization algorithm for modal parameter identification and modal reduction, *Journal of Guidance, Control, and Dynamics*, **8**(5), pp.620-627, 1985.

[12] International Organization for Standardization, Acoustics – Normal equal-loudness-level contours, *ISO 226*, 2003.

[13] Kohnke P.: *ANSYS theory reference*, release 5.3, ANSYS Inc., 1997.

[14] Miller K.: *Measuring the Dynamic Properties of Elastomers for Analysis*, Axel Products, Inc. DynamicRev1, 2000.

Table 1 Cross-section properties of the beams in the full-scale model of the modular joint.

	Middle beam	Support beam	Control beam
Section type (size [mm])	I-shaped (140x80x21x12.5)	I-shaped (120x90x20x12)	Rectangular (80 x 25)
Cross-sectional area [m^2]	4.585×10^{-3}	4.560×10^{-3}	2.000×10^{-3}
Moment of inertia (strong) [m^4]	12.99×10^{-6}	9.632×10^{-6}	1.066×10^{-6}
Moment of inertia (weak) [m^4]	1.807×10^{-6}	2.441×10^{-6}	0.104×10^{-6}
St. Venant's torsion constant [m^4]	5.415×10^{-7}	5.227×10^{-7}	3.543×10^{-7}
Young's modulus [Pa]	2.060×10^{11}	2.060×10^{11}	2.060×10^{11}

Table 2 Spring constants of the bearings in the full-scale model of the modular joint.

	Polyamide bearing (for middle beam)	Rubber bearing (for middle beam)	Polyamide bearing (for support beam)	Rubber bearing (for support beam)	Rubber bearing (control spring)
Vertical [N/m]	5.66×10^8	1.50×10^6	5.97×10^8	5.83×10^6	3.52×10^5
Transverse [N/m]	2.02×10^8	5.07×10^5	0	1.97×10^6	1.19×10^5
Torsion [Nm]	3.94×10^6	9.76×10^3	0	3.89×10^4	2.32×10^3
Rotation [Nm]	2.15×10^5	5.56×10^2	0	2.27×10^3	1.34×10^2

□ : from element test data

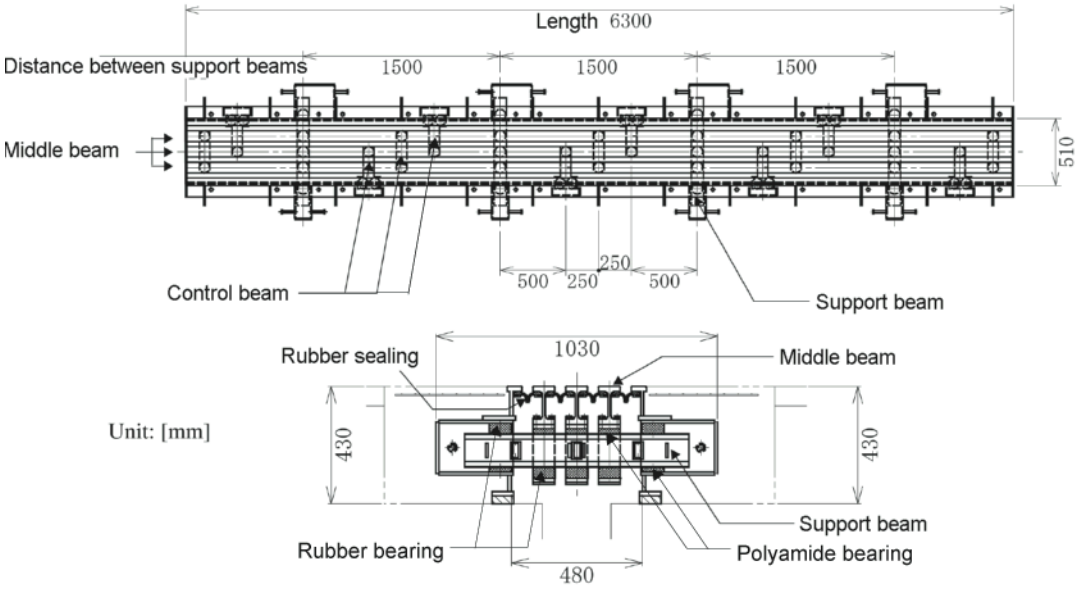

Fig. 1 Plan and cross-sectional views of the full-scale joint model.

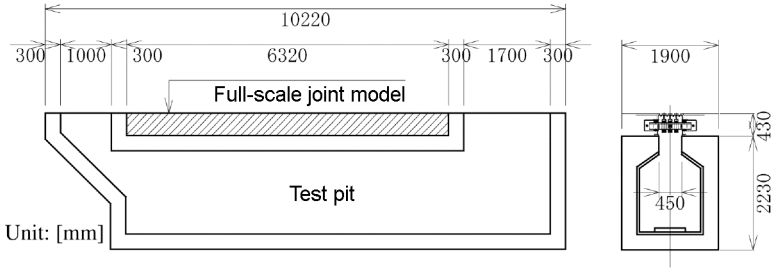

Fig. 2 Cross-sectional views of the test pit.

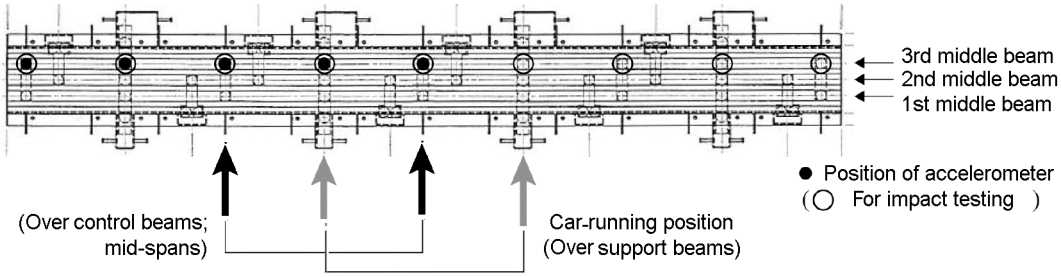

Fig. 3 Positions of car running and vibration measurement.

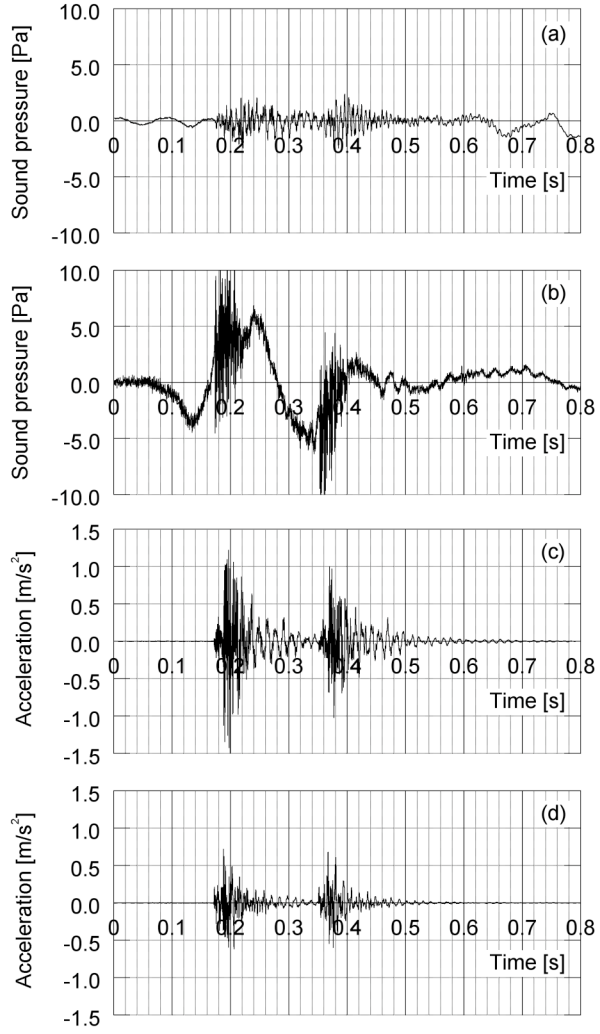

Fig. 4 Example time-series of noise and vibration recorded in the car-running experiment: (a) the noise below the joint; (b) the noise above the joint; (c), (d) the lateral and vertical accelerations of the third middle beam at the center, respectively.

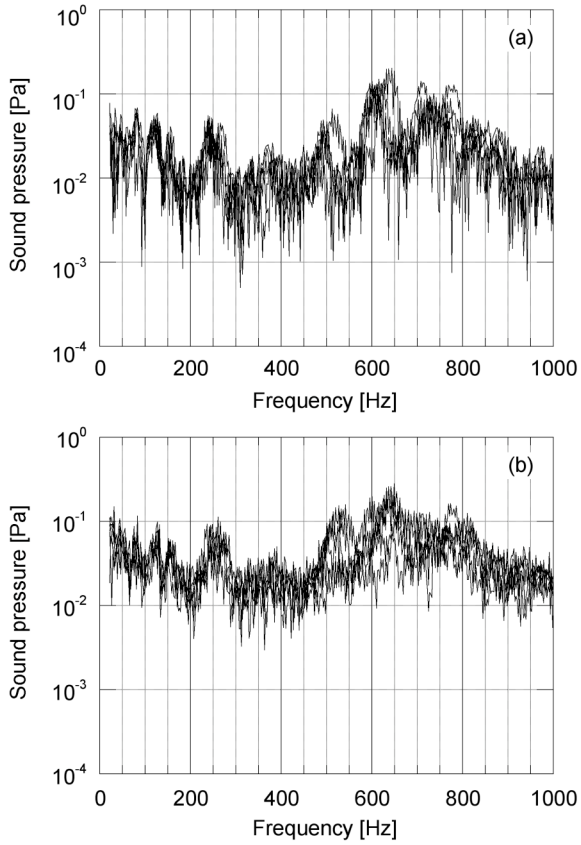

Fig. 5 Spectra of sound pressures above the joint: (a) car running over the control beams; (b) car running over the support beams.

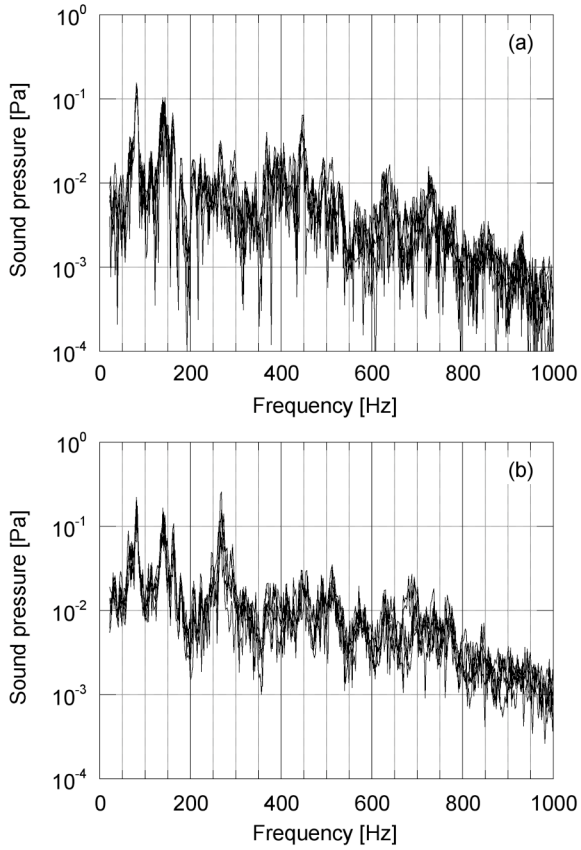

Fig. 6 Spectra of sound pressures below the joint: (a) car running over the control beams; (b) car running over the support beams.

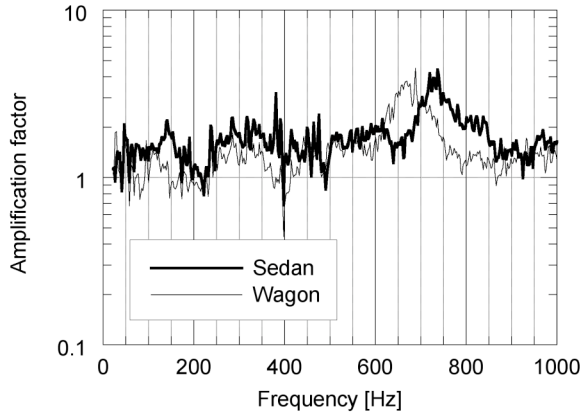

Fig. 7 Acoustic characteristics of the rubber-sealing gap covered by two types of car tire.

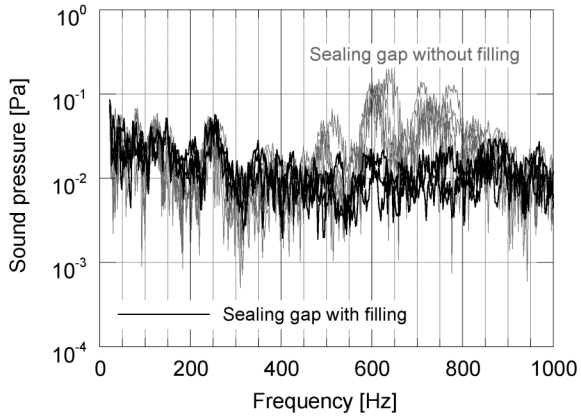

Fig. 8 Comparison of the noise above the joint with and without the fillings for the gaps formed by the rubber sealing with two adjacent middle beams.

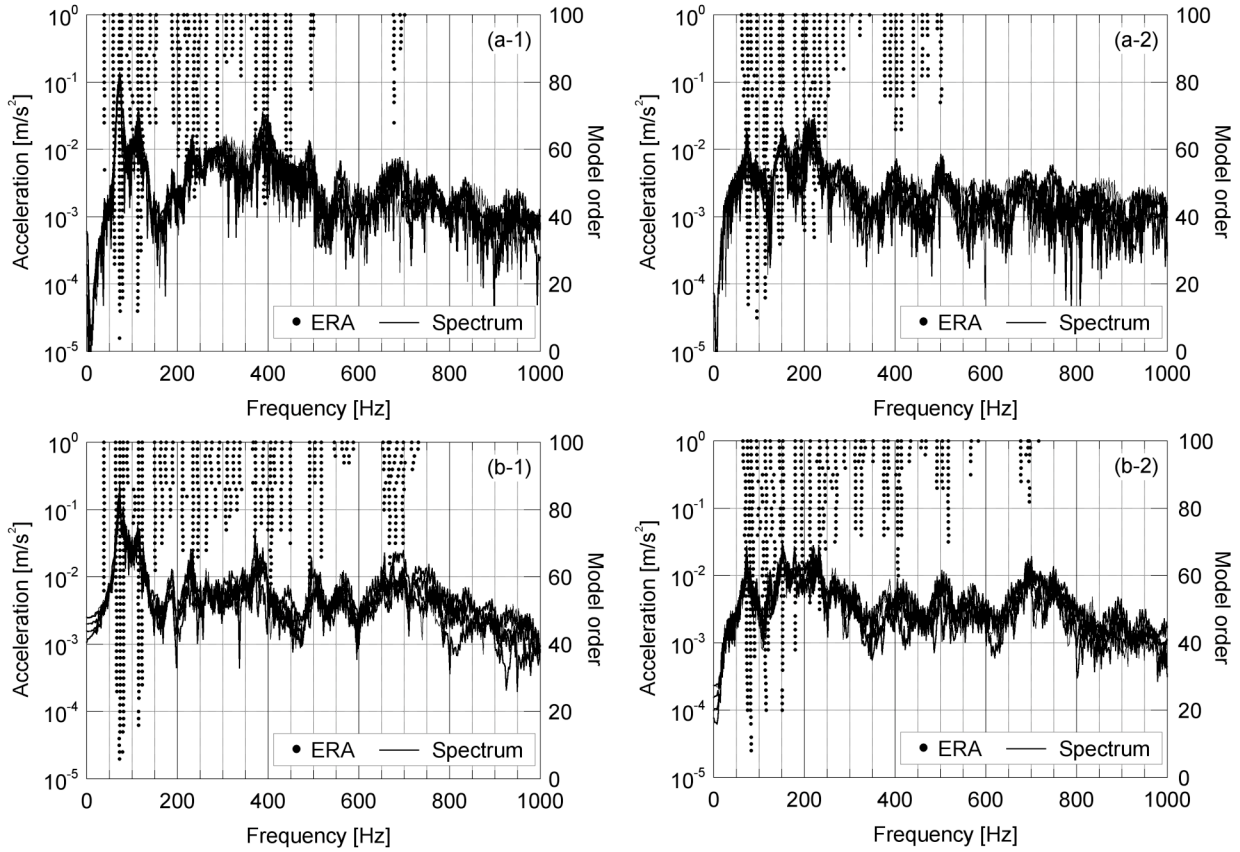

Fig. 9 Spectra of accelerations at the center of the third middle beam and stabilization diagrams (γ > 0.999) of the ERA analysis: (a-1), (a-2) the lateral and vertical accelerations, respectively, for car running over the control beams; (b-1), (b-2) the lateral and vertical accelerations, respectively, for the car running over the support beams.

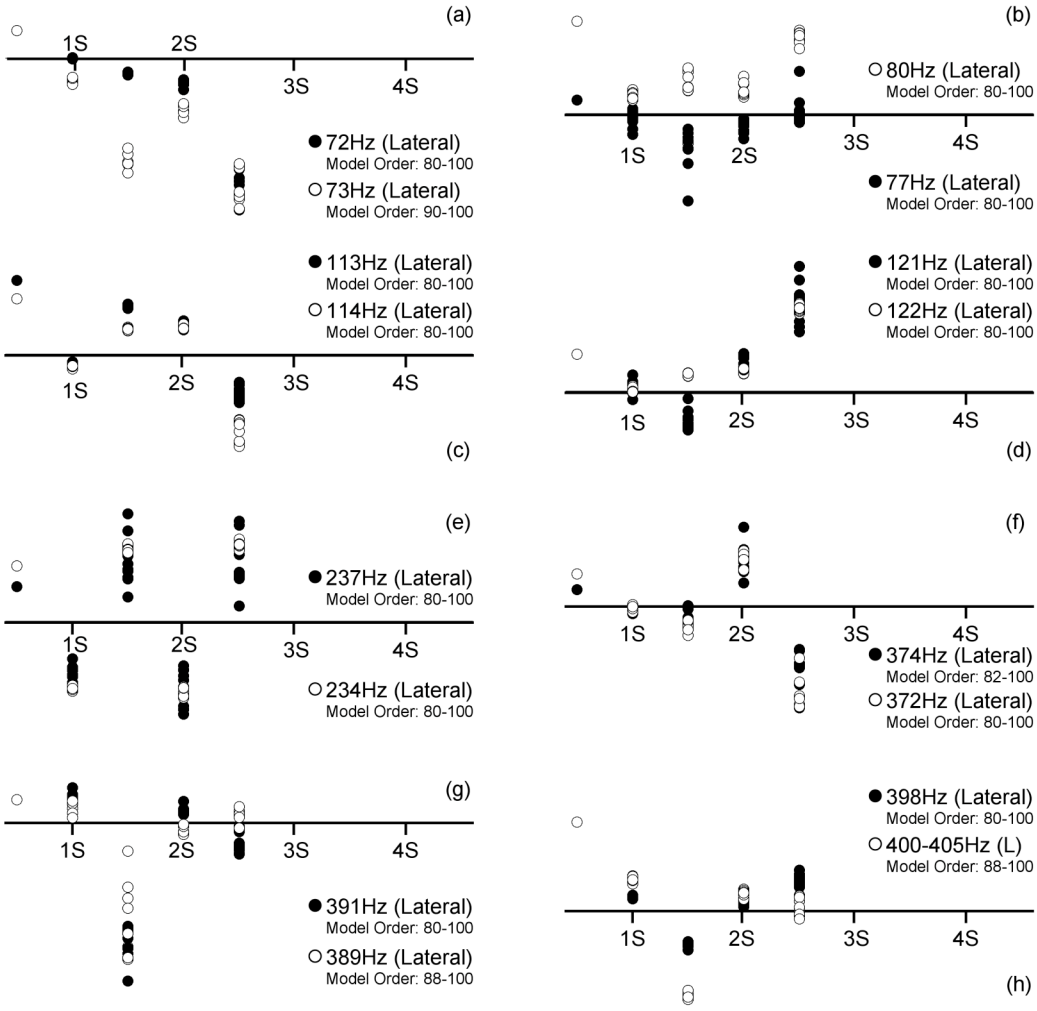

Fig. 10 Lateral vibration modes of the third middle beam, identified by the ERA analysis, corresponding to the dominant frequency components in the cases of the car running over the control beams (•) and over the support beams (◦). '1S' – '4S' indicate the positions of four support beams.

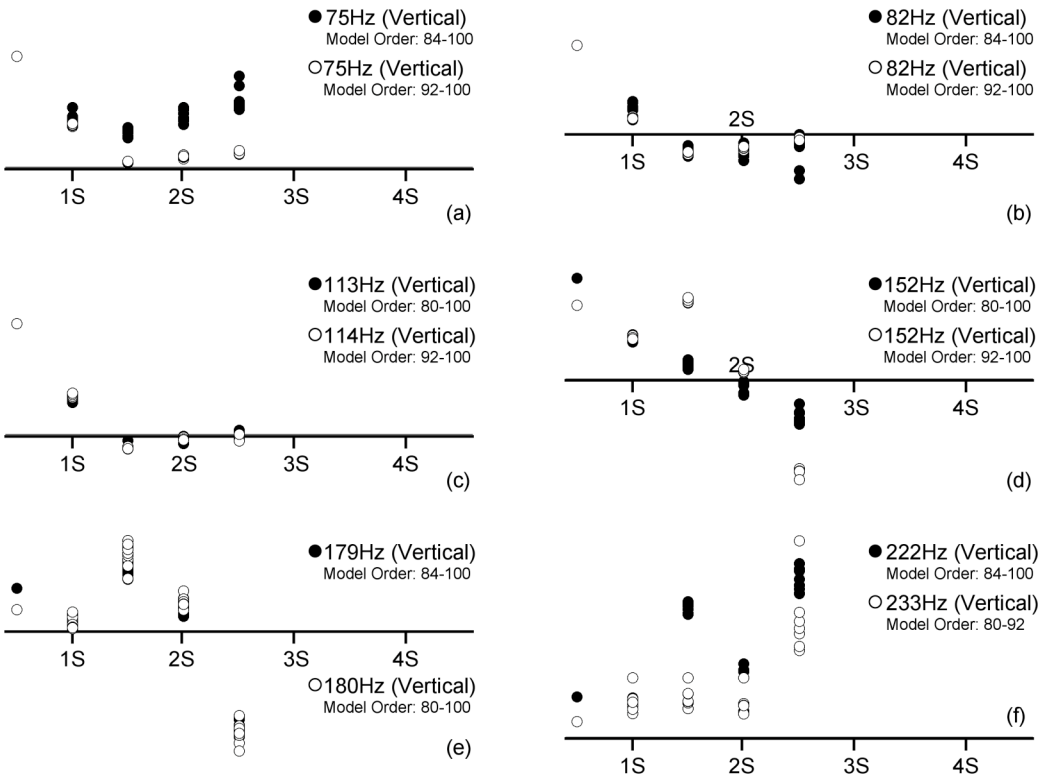

Fig. 11 Vertical vibration modes of the third middle beam, identified by the ERA analysis, corresponding to the dominant frequency components in the cases of the car running over the control beams (•) and over the support beams (◦). '1S' – '4S' indicate the positions of four support beams.

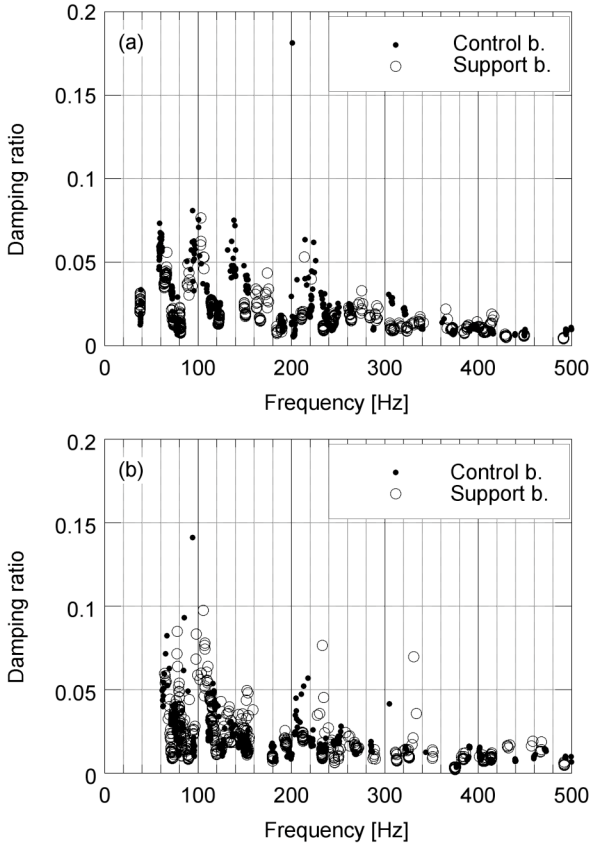

Fig. 12 Modal damping ratio versus frequency identified by the ERA analysis of car-running data (γ > 0.999): (a) the lateral vibration mode; (b) the vertical vibration mode.

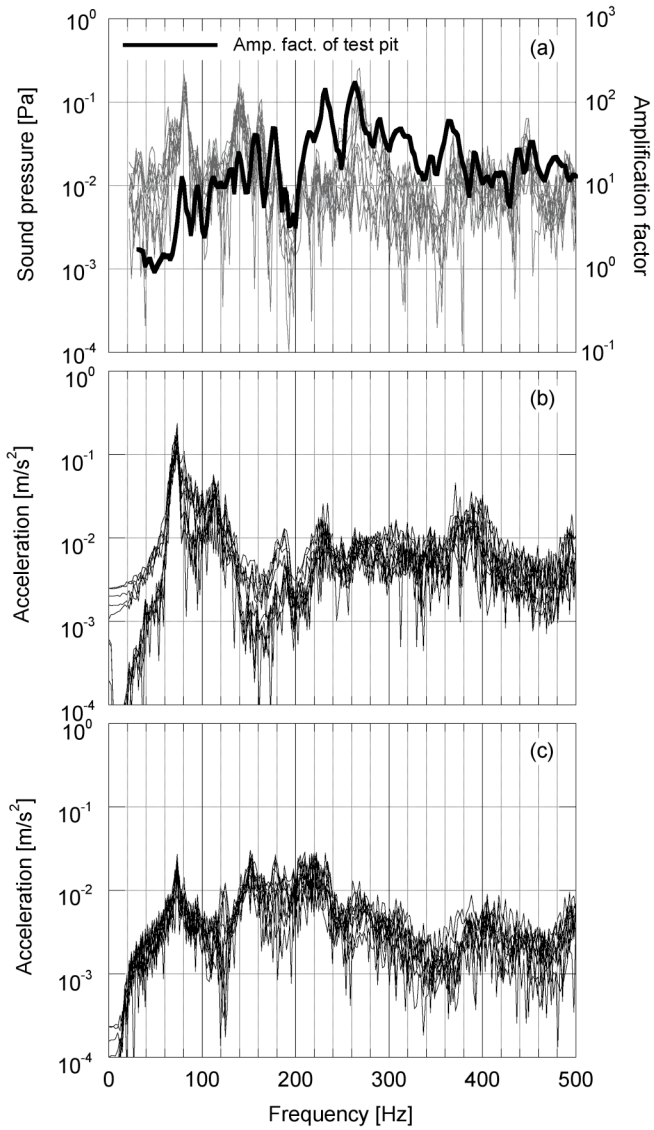

Fig. 13 Comparison of spectra below 500 Hz between the noise below the joint and the accelerations at the middle-beam center: (a) the noises with the acoustic characteristics of the test pit; (b) the lateral accelerations; (c) the vertical accelerations.

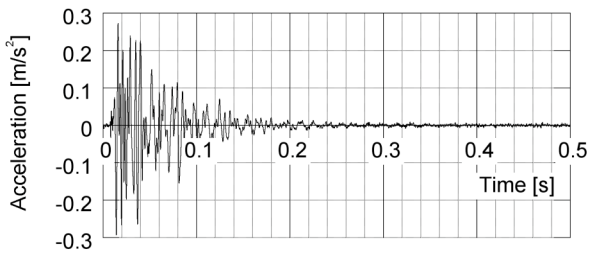

Fig. 14 A time-series of lateral acceleration at the center of the third middle beam in the impact testing.

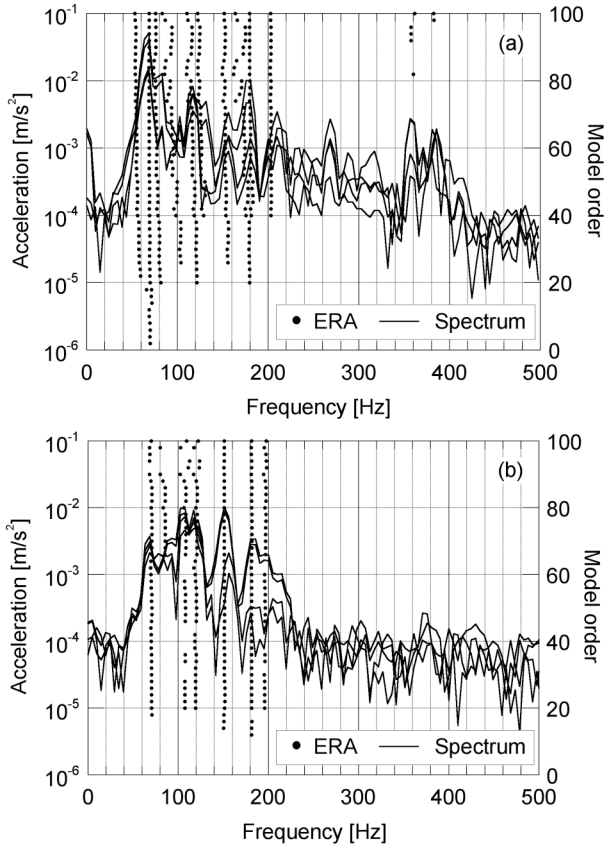

Fig. 15 Spectra of accelerations at the center of the third middle beam and stabilization diagrams ($\gamma > 0.999$) of the ERA analysis: (a) the lateral acceleration for impact in the inclined to the lateral direction; (b) the vertical acceleration for impact in the vertical direction.

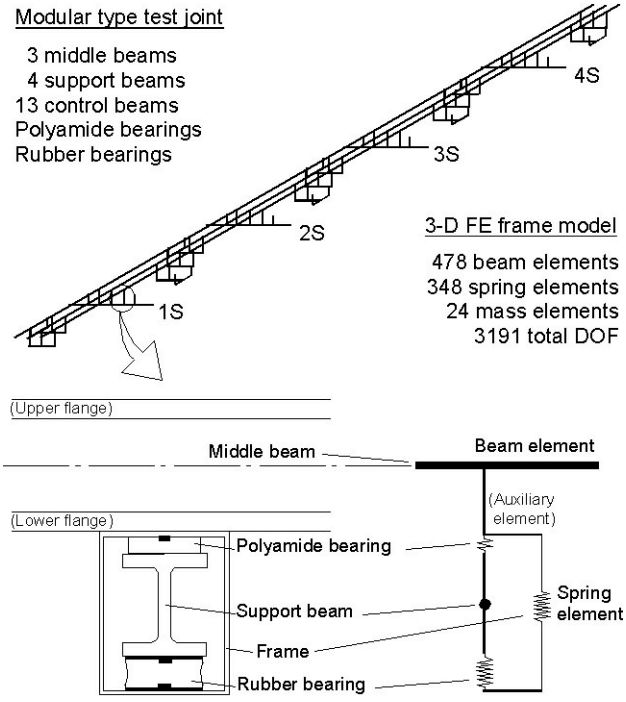

Fig. 16 Three-dimensional finite element frame model of the modular-type test joint.

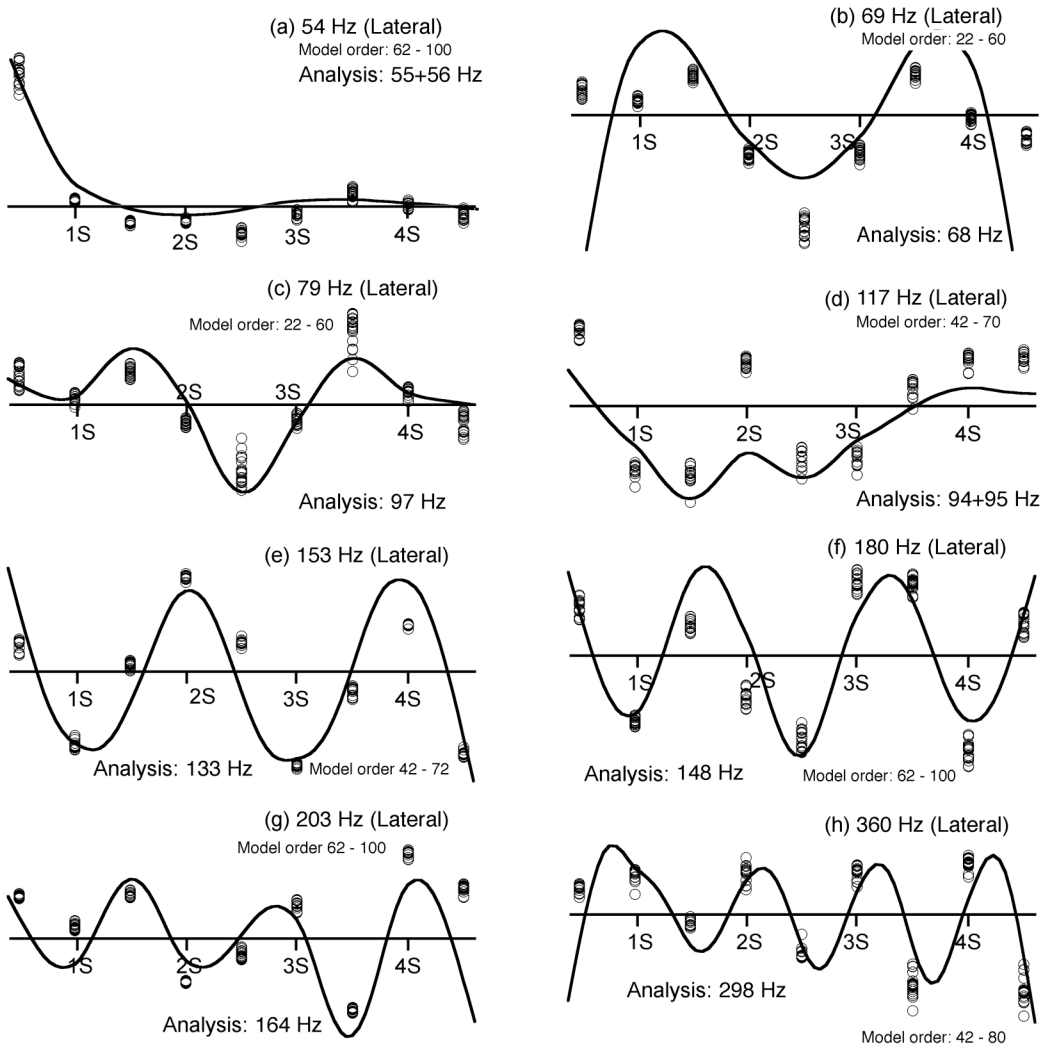

Fig. 17 Comparison between experimentally and analytically identified natural frequencies/ mode shapes in lateral direction.

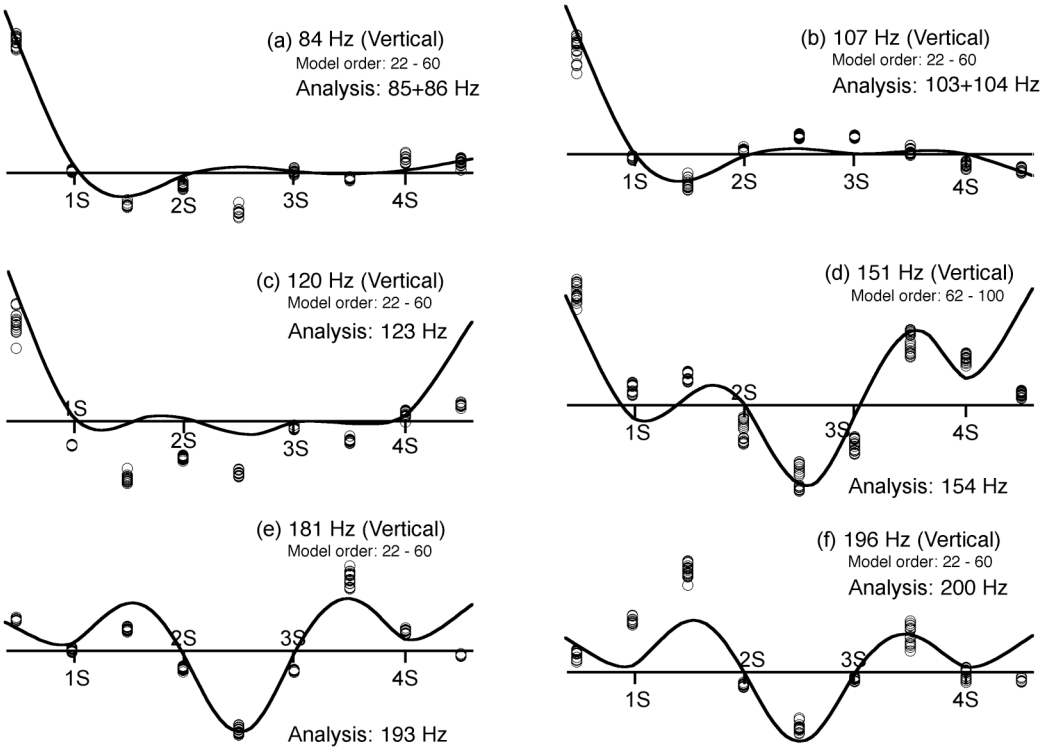

Fig. 18 Comparison between experimentally and analytically identified natural frequencies/ mode shapes in vertical direction.

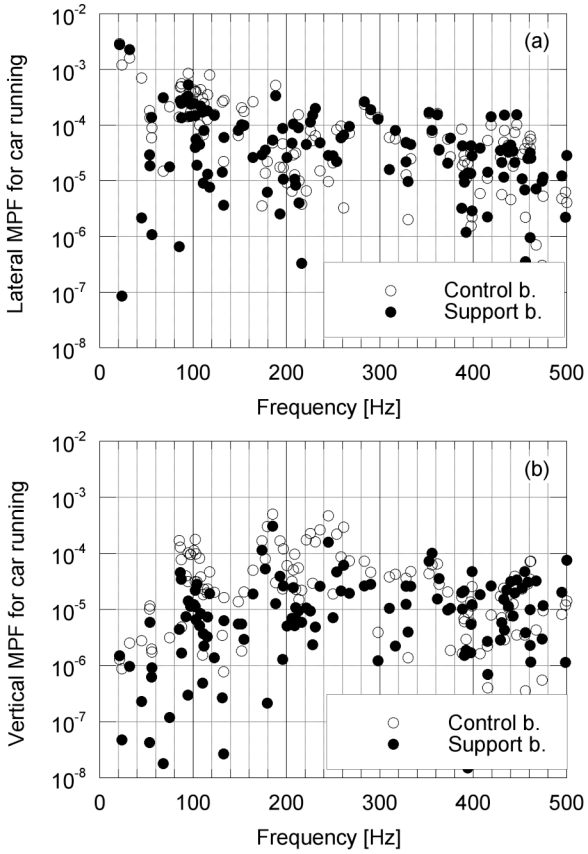

Fig. 19 The modal participation factor for car running versus natural frequency: (a) the lateral impulse forces; (b) the vertical impulse forces.

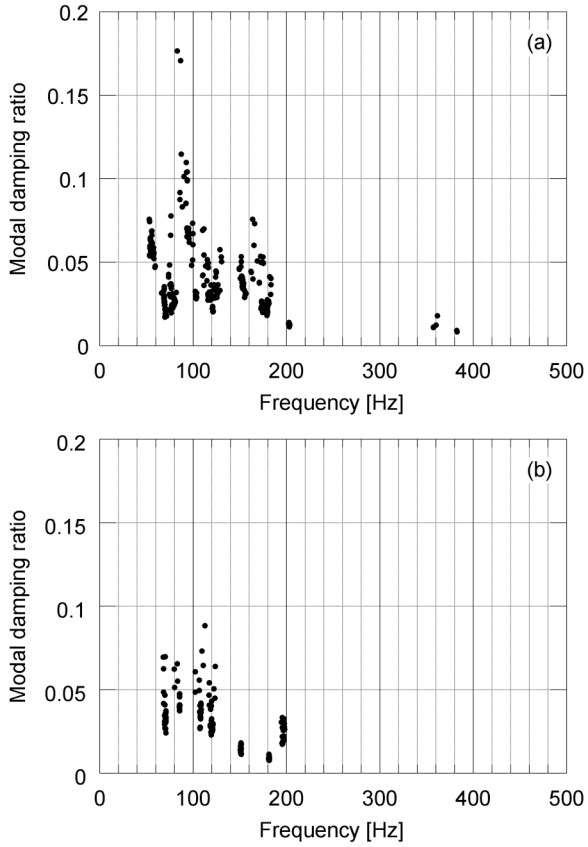

Fig. 20 Modal damping ratio versus natural frequency identified by the ERA analysis of impact testing data ($\gamma > 0.999$): (a) the lateral vibration mode; (b) the vertical vibration mode.

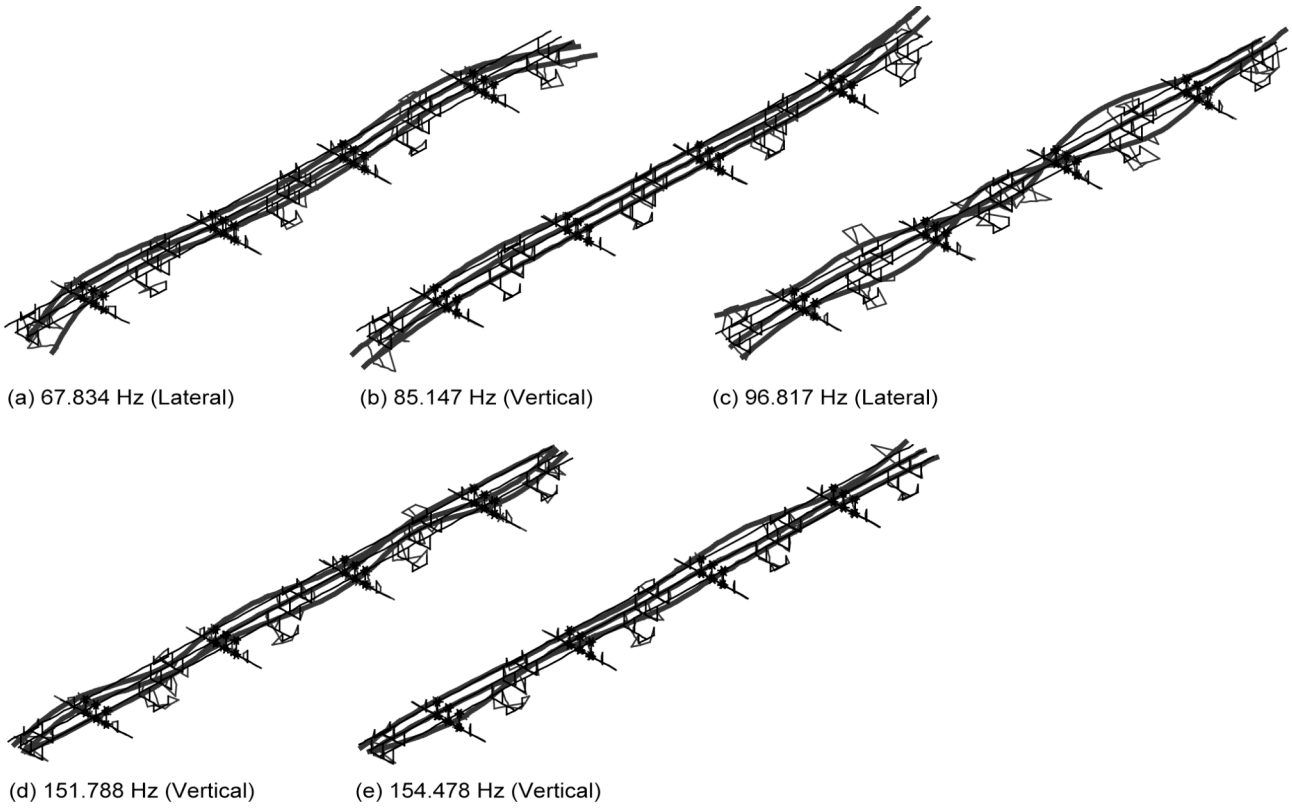

Fig. 21 3D vibration modes of the full-scale model joint (identified by the finite element analysis) corresponding to the noise radiation.